Title: Intranasal Administration of Functionalized Soot Particles Disrupts Olfactory Sensory Neuron Progenitor Cells in the Neuroepithelium

Authors: Jordan N. Norwood[1], Akshay P. Gharpure[2], Raju Kumal[2], Kevin L. Turner[3], Lauren Ferrer Pistone[4], Randy Vander Wal[2], Patrick J. Drew[1,3,4,5]

Affiliations:

1. Cell and Developmental Biology Graduate program

2. The EMS Energy Institute, and Departments of Energy and Mineral Engineering, Materials Science and Engineering, and Mechanical Engineering

3. Department of Biomedical Engineering

4. Department of Engineering Science and Mechanics

5. Department of Neurosurgery

Pennsylvania State University, University Park PA 16802

Correspondence to pjd17@psu.edu or ruv12@psu.edu

Acknowledgements: This work supported by an PSU Institute of Energy and Environment seed grant to RVW and PJD, F31NS105461 to JNN, and R01NS078168 to PJD.

Competing Interests: None

Abstract: Exposure to air pollution has been linked to the development of neurodegenerative diseases and anosmia, but the underlying mechanism is not known. Additionally, the loss of olfactory function often precedes the onset of neurodegenerative diseases. Chemical ablation of olfactory sensory neurons blocks the drainage of cerebrospinal fluid (CSF) through the cribriform plate and alters normal CSF production and/or circulation. Damage to this drainage pathway could contribute to the development of neurodegenerative diseases and could link olfactory sensory neuron health and neurodegeneration. Here, we investigated the impact of intranasal treatment of combustion products (laboratory-generated soots) and their oxygen functionalized derivatives on mouse olfactory sensory neurons, olfactory nerve cell progenitors, and the behavior of the mouse. We found that after a month of every-other-day intranasal treatment of soots, there was minimal effect on olfactory sensory neuron anatomy or exploratory behavior in the mouse. However, oxygen-functionalized soot caused a large decrease in globose basal cells, which are olfactory progenitor cells. These results suggest that exposure to air pollution damages the olfactory neuron progenitor cells, and could lead to decreases in the number of olfactory neurons, potentially disrupting CSF drainage.

Introduction

Air pollution, particularly small combustion particles (<2.5 μm, $PM_{2.5}$), is a large contributor to global mortality (Burnett et al., 2018). These small particles are produced by combustion in internal combustion engines, jet aircraft engines, and during cooking. Once generated, these particles can be oxidized over time (Rattanavaraha et al., 2011; Li et al., 2013; Pourkhesalian et al., 2015), generating surface functionalized oxygen groups which can increase their cellular toxicity (Li et al., 2009; Holder et al., 2012; Li et al., 2013).

In addition to the many other adverse health effects of air pollution, there is a strong epidemiological link between exposure to air pollution, particularly $PM_{2.5}$, to the development of neurodegenerative diseases (Wang et al., 2017; Forman and Finch, 2018; Peters et al., 2019) and to mental disorders (Atanasova et al., 2008; Hummel et al., 2017; Buoli et al., 2018). Exposure to air pollution, particularly fine particulate matter ($PM_{2.5}$), also leads to reduced sense of smell and anosmia (Ajmani et al., 2016a; Ajmani et al., 2016b) and can damage nasal tissue (Calderon-Garciduenas et al., 2003). Interestingly, anosmia and a decline of sense of smell precede the onset of neurodegenerative disorders (Doty, 1989; Wilson et al., 2009; Rahayel et al., 2012; Growdon et al., 2015; Ottaviano et al., 2016; Roberts et al., 2016; Murphy, 2019) and is also associated with depressive disorders (Croy et al., 2014; Kohli et al., 2016). Similar damage and sensory deficits have been implicated in COVID-19 pathology (Cooper et al., 2020). The observed associations between particulate exposure, decreased olfactory function, and development of neurodegenerative and mental disorders suggests that some of the observed degeneration might originate from the damage to olfactory sensory neurons (OSNs) in the nasal epithelium.

The movement of cerebrospinal fluid (CSF) is thought to remove waste from the brain (Iliff et al., 2012; Nedergaard, 2013), and disruption of normal CSF turnover and circulation has been hypothesized to lead to the development of neurodegenerative diseases (Albeck et al., 1998; Stoquart-ElSankari et al., 2007; Simon and Iliff, 2016; Benveniste et al., 2017). In addition to CSF drainage pathways through meningeal lymphatics and arachnoid granulations (Boulton et al.,

1996; Aspelund et al., 2015; Louveau et al., 2016; Absinta et al., 2017; Ma et al., 2017; Ma et al., 2018), CSF is known to drain out of the cranial compartment via the cribriform plate, the perforated bone between the olfactory bulbs and nasal cavity (Bird et al., 2018), in both humans (de Leon et al., 2017) and animals (Bradbury et al., 1981; Mollanji et al., 2002; Nagra et al., 2006; de Leon et al., 2017; Norwood et al., 2019). The level of amyloid beta oligomers in this discharge is correlated with the severity of cognitive decline (Yoo et al., 2020). The fluid flows in-between olfactory neuron axons, and chemical ablation of OSNs blocks this normal outflow, leading to decreased CSF production and/or altered CSF circulation (Norwood et al., 2019). Thus, any damage to olfactory sensory neurons by air pollutants, in addition to impairing the sense of smell, might lead to disruption of normal CSF circulation which can then contribute to the development of neurodegenerative diseases.

Olfactory sensory neuron cell bodies are located in the nasal epithelium and send their axons to the olfactory bulb through the holes (foramina) in the cribriform plate. Because these neurons are exposed to the environment, they have a relatively short lifetime (several months (Gogos et al., 2000)), and are constantly replenished throughout the lifetime of the organism. Olfactory sensory neurons are generated from a population of nearby stem cells (Brann and Firestein, 2014; Liberia et al., 2019), and the ongoing neurogenesis of olfactory sensory neurons continues throughout the life of the animal. There are two classes of stem cells in the nasal epithelia that give rise directly and indirectly to OSNs, horizontal basal cells (HBCs) and globose basal cells (GBCs) (Child et al., 2018). GBCs generate olfactory sensory neurons, while HBCs are usually quiescent and are involved in regenerating the nasal epithelial in response to injury. The capacity for regeneration has limits and is reduced with aging or repeated insults (Child et al., 2018). Chronic nasal inflammation causes degeneration of olfactory neurons and their progenitor cells in both humans and animals (Chen et al., 2019; Hasegawa-Ishii et al., 2019). Insults that kill olfactory sensory neurons and their progenitor cells will lead to shrinkage and loss of the nasal

CSF outflow pathways. Insults that kill either GBCs or HBCs will decrease the population of stem cells, potentially resulting in a decrease in the number of OSNs later in life.

To better understand the effects of air pollution on olfactory sensory neurons and their progenitor cells, we investigated the impact of intranasal treatment with surrogates for combustion generated 'soots' synthesized from carbon black precursors. Carbon black is primarily composed of elemental carbon, but like combustion-produced soot, it is formed by the partial combustion or thermal decomposition of hydrocarbons (Donnet, 1993). The morphology consists of primary particles that are partially merged or appear "fused" into aggregates (Fig. 1A). Such synthetic soots are also free of variable combustion-derived contaminants such as metals, ash, or condensed organics. We treated the mice with either non-functionalized soots, which resemble the combustion products immediately after their production, or functionalized soots that have been subject to oxygen functionalization, modifying their surface chemistry, mimicking the oxidation processes that would take place during atmospheric aging. We found that relative to vehicle controls, neither non-functionalized soots nor oxygen-functionalized soots had appreciable impact on olfactory sensory neurons. The effects of soot exposure on exploratory behavior was also minimal. However, oxygen-functionalized soots greatly decreased the levels of olfactory progenitor cells, suggesting that exposure to these particles can set up a long-term decrease in the number of OSNs. Such a decrease could lead to anosmia and decreased CSF movement.

Methods

Synthesis of soots: Synthetic soot was produced by functionalizing commercial carbon black, (Regal 250, Cabot Corp.). Carbon black was selected for its chemical purity and size similarity to diesel engine-produced soot. To introduce oxygen functional groups such as phenol, carboxyl and carboxylic, we used wet-chemical treatment based on acid etching (Romanos et al., 2011). In this preparation a gram of carbon black was treated with 100 mL laboratory grade concentrated nitric

acid (HNO_3, > 90%) under reflux for a duration of 24 hours at 80˚C, just below the acid's boiling point of 83˚C. The carbon-acid mixture was continuously stirred using a magnetic stirrer to ensure uniform exposure and functionalization. The mixture was maintained at a consistent simmer and was thereafter washed with distilled water, filtered, and dried to obtain functionalized carbon black as a synthetic, oxidized soot. Any potential residual organic or aromatic compound present on the manufactured material as supplied would be oxidized and removed under these conditions.

Characterization of soots: To visualize soot particles, we used transmission electron microscopy (FEI Talos F200X instrument equipped with Quad element EDS detector capable of both transmission electron microscopy (TEM) and scanning transmission electron microscopy (STEM)). For imaging, a beam acceleration voltage of 200 keV was used. Beam current was kept less than 5 nA for which sample damage or alteration is negligible at these magnifications (< 120 kX). Image defocus was one or two steps before the eucentric position. Images were captured using a Ceta-cooled CCD. Samples were dispersed and sonicated in methanol before being dropped onto 300 mesh C/Cu lacey TEM grids. High angle dark field (HAADF) images were obtained using an annular detector. EDS for elemental analysis and mapping was performed in the TEM. We also used the STEM mode, which has a high spatial resolution on the order of the minimum probe size (1.6 Å). The instrument was fitted with a 4-quadrant SDD Super-X EDS detector for EDS. The detection limit is typically < 1 atomic percent (at. %) depending on collection parameters. Typically, 7–10 regions of each material (nascent and functionalized forms) were sampled to gauge elemental representation. EDS was performed in STEM mode with a sample holder designed to provide low background signal for EDS. XPS experiments were performed using a Physical Electronics VersaProbe II instrument equipped with a monochromatic Al K_α x-ray source (hν = 1,486.7 eV) and a concentric hemispherical analyzer. Charge neutralization was performed using both low energy electrons (< 5 eV) and argon ions.

Peaks were charge referenced to C-C band in the carbon 1s spectra at 284.5 eV. Measurements were made at a takeoff angle of 45° with respect to the sample surface plane. This resulted in a typical sampling depth of 3-6 nm (95% of the signal originated from this depth or shallower). Quantification was done using instrumental relative sensitivity factors (RSFs) that account for the X-ray cross section and inelastic mean free path of the electrons. A Thermogravimetric Analyzer (TA 5500, TA instruments) coupled to a Discovery Mass Spectrometer (MS) was used to analyze mass loss and the composition of the evolved gases as a function of temperature. The temperature was ramped up at 5˚C/min in an inert atmosphere. The TGA features low volume, maximum temperature to 1200˚C and has an inert quartz liner. The MS is a quadrupole mass spectrometer with a heated capillary interface, offering a 1-300 AMU range, unit m/z resolution. A Horiba LabRam Raman microscope was used to obtain Raman spectra for the samples when exposed to a 488 nm 100 mW laser with a 300 grooves/mm grating, providing a spectral resolution of 4 cm^{-1}.

XPS was applied to dispersed powder to quantify both surface oxygen atom content (at. % basis) and distribution of oxygen functional groups (-C-OH, phenolic, -C=O, carbonyl, and -COOH, carboxylic), the nominal C1s (energy loss) positions were 286, 287 and 288.5 keV. CASA was applied to deconvolve the high-resolution spectra, with group contributions ratioed to the total oxygen elemental content. As a baseline, nascent (untreated) carbon black was also subject to the same analytical procedure as a “blank” sample. Wet acid reflux treatment of carbon black yielded ~31 atomic % (near-surface) oxygen compared to the untreated carbon black, registering negligible surface content, (<1 at. %). By curve-fitting the C1s spectral loss profile, the calculated distribution across function groups was determined as 10.2% (phenolic, C-OH); 4.9% (carbonyl, C=O); and 9.4% (carboxylic, -COOH) (Vander Wal et al., 2011). (The good agreement (± 10%) in the measured and calculated value of atomic oxygen indicates appropriate curve fitting for functional group identification.) The TGA curve shows distinct regions of mass loss owing to functional groups leaving as temperature increases. The 5 wt.% net mass loss corresponds to the

gasification of the carbon by the chemisorbed oxygen groups. Resolved by temperature, the TGA spectrum supported XPS identification of functional groups by successive mass loss stages for the oxygen group classes. Temperature resolved mass loss curves reveal m/z peaks at 44 AMU (CO_2) arising predominantly from carboxylic groups and at 28 AMU (CO) arising from carbonyl and phenol groups (Kundu et al., 2008).

Soot treatment protocol for mice: After the mouse had been rendered unconscious by a brief exposure to isoflurane, 20 µL of soot (functionalized or non-functionalized, 1% in sterile H_2O) or vehicle control (sterile H_2O) was administered to the left nare dropwise using a pipette. The animal was then inverted to allow for excess fluid to exit the nasal cavity. This treatment was repeated every other day (3 days a week) for one month. The animals were monitored and weighed daily after treatment.

Histology: Mice were sacrificed via isoflurane overdose and perfused intracardially with heparinized-saline followed by 4% paraformaldehyde. The heads were fixed in 4% paraformaldehyde for 24 hours, decalcified for 48 hours in formic acid (4M) solution, and saturated in 30% sucrose for sectioning. Tissue sections of 100 µm thickness were sectioned on a freezing microtome. All staining was done in 24 well plates, with one section per well. Primary antibodies (and their respective dilutions) used on tissue sections were as follows: OMP (WAKO Chemicals U.S.A, 1:500), Pax6 (Santa Cruz, 1:250), and p63 (Abcam, 1:500). Sections were incubated in the primary antibody solution (primary antibodies + PBS-Triton) overnight at 4˚C. Sections were then incubated in secondary antibody solution (secondary antibodies + PBS-Triton) for one hour at room temperature. The following secondary antibodies were purchased from Abcam and used at a 1:500 working dilution: Goat Anti-Rabbit IgG H and L (Alexa Fluor 488), Donkey Anti-Goat IgG H and L (Alexa Fluor 488), Goat Anti-Mouse IgG H and L (Alexa Fluor 488), Donkey Anti-Rabbit IgG H and L (Alexa Fluor 647), Donkey Anti-Goat IgG H and L (Alexa

Fluor 647), and Goat Anti-Mouse IgG H and L (Alexa Fluor 647) preabsorbed. Sections were mounted on silane-coated unifrost slides (Azer Scientific), then cover slipped using fluoroshield mounting medium with DAPI (Abcam). Imaging was done on an Olympus Fluoview 1000 confocal and images were processed using ImageJ (NIH).

Cell quantification procedures: To quantify the mean fluorescence of Pax6 and p63 antibody expression, images were first obtained on the Olympus FluoView 1000 confocal. Imaging settings were kept constant across samples to enable quantification of fluorescence. Using ImageJ (NIH), a rectangular ROI was drawn (250 μm in width and 50 μm in height) along the apical side of the neuroepithelium. For every animal, the ROI was drawn 250 μm in the rostral direction from the cribriform plate within the neuroepithelium located on the dorsal side of the medial olfactory nerve. The mean fluorescence of the ROI for each color channel (corresponding to each of the antibodies used) was obtained and averaged together for each treatment group. Data was plotted and analyzed in GraphPad Prism 8, using one-way ANOVA to test for significance.

Quantification of mouse locomotion and rearing behavior: To measure any effects of intranasal soot treatment on behavior, mice were individually placed in a 34 x 31 x 14 cm (L x W x H) plastic box one month after the start of the treatment. All experiments were performed between 900 and 1600 ZT. The acquisition and analysis were done with the experimenter blinded to the treatment, and the order of animals was randomized. Mice were placed in the enclosure for 20 minutes, and the behavior was quantified over this entire period. The enclosure was cleaned with 70% ethanol between mice. The amount of locomotion and rearing behavior were monitored using an Intel® RealSense™ Depth Camera D435 (Hong et al., 2015). This camera provides simultaneous visible light and depth information used to calculate the animal's distance from the camera. Images were acquired at a nominal rate of 15 frames/second using MATLAB (https://github.com/IntelRealSense/librealsense). To track the distance the animal traveled, the

distance between the centroid of the mouse was calculated between each successive frame. This distance between frames is then summed over the course of the 20 minutes. Rearing events were defined as when the mean of the highest 20% of pixels of the mouse exceeded 8 cm from the bottom of the enclosure.

A generalized linear mixed-effects model (MATLAB function *fitglme*) was used to evaluate the differences in rearing events, rearing duration, and distance traveled. Each treatment (vehicle, non-functionalized and functionalized soot) was a fixed-effect, with the sex treated as a random effect.

Data availability: Code for the acquisition, analysis and plotting of the behavioral data, as is the behavioral data plotted in figure 4, is available here: https://github.com/DrewLab/Norwood_Gharpure_Turner_Ferrer-Pistone_VanderWal_Drew_Manuscript2020

Results

Characterization of soot compounds

Transmission electron micrograph of a carbon black aggregate and primary particle is shown in Fig. 1. The aggregate consists of pseudo-spherical primary particles, partially merged or fused together forming a fractal aggregate. A Raman spectrum of the nascent carbon black is shown in Fig. 1c. Raman spectroscopy has been developed as a standard method for determining the planar coherence lengths (L_a) in graphitic carbon, which possesses limited long-range order (Tuinstra and Koenig, 1970). The lower frequency "D" peak at ~1360 cm^{-1} arises from disorder-induced Raman activity of zone-boundary A_{1g} phonons whereas the "G" peak at ~1580 cm^{-1} reflects the in-plane stretching motion of the aromatic rings, designated as E_{2g} motions. Their comparable intensity reveals considerable disordered carbon, characteristic of furnace blacks and representative of combustion-produced soot emissions (Dennison et al., 1996; Sadezky et al.,

2005). Their intensity ratio is an accepted technique for determining L_a in disordered graphitic materials, given by the relation $4.4(I_d/I_g)^{-1} = L_a$, calculated here as 0.85 nm, a value commensurate with the short lamellae viewed by HRTEM (Sadezky et al., 2005). The asymmetry of the D-peak due to the extended low frequency (shift) tail is consistent with further disorder of the carbon lattice such as sp^3 and sp^2 carbon at the periphery of the crystallites, contributing vibrations of A_{1g} symmetry (Sadezky et al., 2005; Parent et al., 2016). Fluorescence from the oxygen groups and their auxochromic interactions with the π electrons of the sp^2 carbon network dwarfed the Raman signature of the functionalized material, preventing its comparison to the nascent material.

Figure 1D shows a high angle dark field TEM image of soot particles for reference and respective EDS map displaying carbon (blue) and oxygen (red) for the nitric acid functionalized carbon black. While EDS cannot point to a definitive volumetric vs. surface oxygen presence given its 2-D nature, nitric acid–treated carbon black shows oxygen appearing to be concentrated along the particle perimeter, reflecting a higher near-surface contribution near the particle edge along

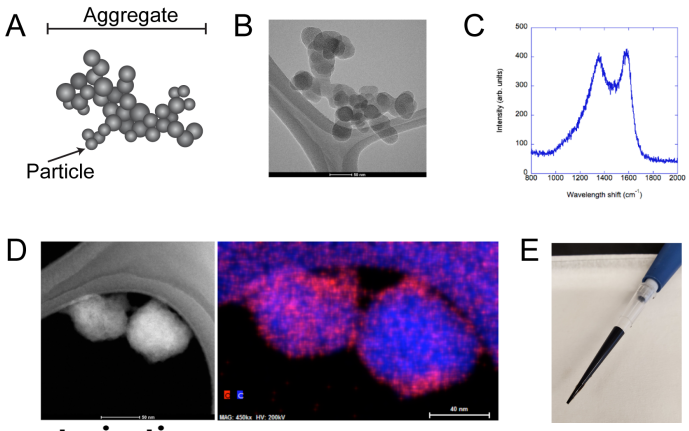

Figure 1: Soot characterization
A) Schematic showing the structure of a soot particle, which is an aggregate of smaller particles. B) TEM image of a soot aggregate supported by the lacy mesh of the TEM grid, illustrating the morphological structure of the particles. Pseudo-spherical primary particles are coalesced, forming a branched aggregate whose 2D projection is shown in the image. C) Raman spectrum of R-250 carbon black. The two peaks of similar intensity are indicative of unstructured (non-graphitic) carbon. D) Left, a high angle, annular dark field (HAADF) image of soot particles. Formed by scattered (rather than transmitted) intensity, the uniformity illustrates the lack of crystallinity and absence of heavy elements such as metals. Right, corresponding energy dispersive spectroscopy (EDS) map. The elemental map reveals the spatial distribution of carbon and oxygen, integrated through the particle. The higher intensity at the particle perimeters shows that the oxygen is at the particle surfaces. The grid lacy mesh appears as arched support). E) Photograph of suspended soot (1%) in water. The oxygen surface functionalization makes the particle hydrophilic, enabling stable dispersion in aqueous media.

the beam path. In the 2-D image it must be noted that EDS shows relative amounts of elemental carbon and oxygen and does not give information on what functional groups are present. An image of the 1% solution of soot in water that is applied intranasally is shown in Figure 1E.

Soot accumulates in the nasal passageway and lungs, but does not change the structure of the olfactory nerve or OSNs

We treated mice intranasally with vehicle, non-functionalized soot, or functionalized soot for one month. Mice were briefly anaesthetized with isoflurane and an intranasal solution of soot (functionalized or non-functionalized, 1% in sterile water) or vehicle (sterile H2O) was administered to the left nare. This treatment was repeated every other day (three times a week) for one month. We saw no appreciable differences between weight of mice of the different treatment groups (data not shown). After sacrifice, the skulls were rapidly decalcified (Norwood et al., 2019) and sectioned. Examples of thin sections of olfactory bulb/nasal cavity area are shown in Fig 2A-C, and accumulation of functionalized soot in the olfactory epithelium, but not non-functionalized soot was observed. Soot could be seen in the lungs of treated animals (Fig 2D-F). A total of 0.2mg of soot particles was applied each day, though we conservatively estimate that < 20% remained in the nose after inverting the mouse. Given that an average mouse respiratory

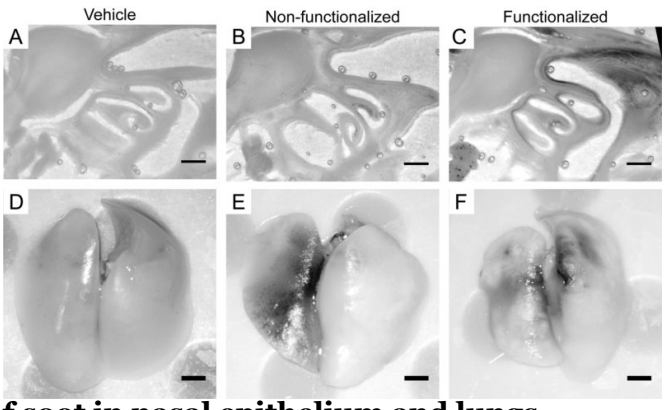

Figure 2: Uptake of soot in nasal epithelium and lungs
Images of sagittal sections of decalcified skull and nasal epithelium after one month of treatment with a vehicle (A), non-functionalized soot (B) and functionalized soot (C). Images of the lungs of vehicle-treated (D), non-functionalized (E) and functionalized soot-treated (F) mice. Only the functionalized soot shows appreciable accumulation in the nasal epithelium, though both soot types accumulate in the lungs. All scale bars 1 mm.

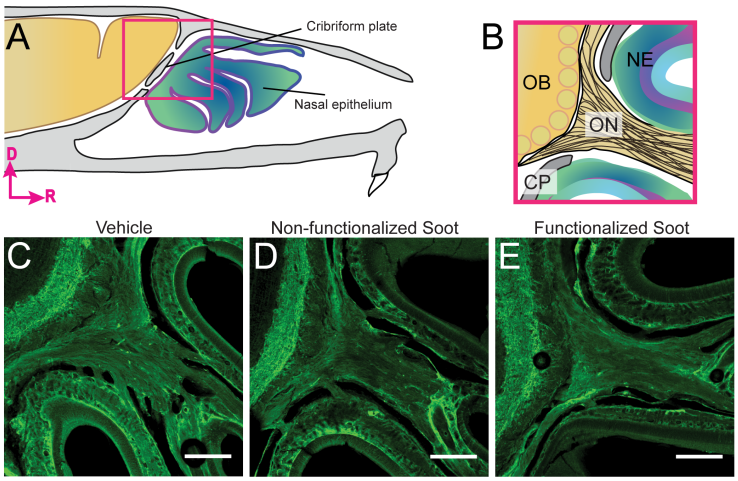

Figure 3: Soot treatment does not affect olfactory sensory neurons
A) Schematic showing sagittal cross-section of the mouse skull. Olfactory nerve (ON), neuroepithelium (NE), cribriform plate (CP), olfactory bulb (OB). B) Enlargement of box in A), showing the olfactory bulb, cribriform plate and foramina where the olfactory nerve enters the brain from the nasal cavity. Glomeruli are yellow circles. Example images of sagittal sections of the olfactory nerve location shown in B) from mice treated with vehicle (C), non-functionalized soot (D), and functionalized soot (E). Scale bar 250 μm.

volume over a day is ~34.5 L (0.15 mL tidal volume with 160 breaths a minute (Zhang et al., 2019)) this works out an effective dose equivalent to breathing air with a $PM_{2.5}$ level of ~300 μg/m^3, comparable to the air quality in Beijing (Zíková et al., 2016) or New Delhi (Pant et al., 2017).

We also examined the status of olfactory sensory neurons to see if either type of soot had a detectable effect on their health. To assess any damage to the olfactory bulb or nerve caused by exposure to the soot particles, the area was examined histologically utilizing rapid decalcification and sectioning. Olfactory sensory nerves enter the cranial compartment through the cribriform plate (Bird et al., 2018). We visualized the nerve in soot and vehicle-treated mice using an antibody against olfactory marker protein (OMP) (Fig. 3). We found no discernable difference in olfactory nerve labeling among the treatments, indicating that soot treatment does not have any obvious effect on olfactory sensory nerves for the treatment duration used. This is markedly different from intranasal treatment with zinc sulfate, a single treatment which causes the rapid and irreversible ablation of olfactory sensory neurons (Norwood et al., 2019).

Effects of intranasal soot treatment on exploratory behavior

One important question is to what extent soot treatment impacts the behavior of the mice. We quantified locomotion and rearing behavior using an Intel RealSense D435 depth-sensing camera (Hong et al., 2015) after intranasal soot exposure (Fig. 4). Treated mice from all three treatment groups were individually placed in a novel environment (white plastic container) after the one month of treatment and their movement and rearing behaviors were monitored for 20 minutes. Rearing behavior is a measure of anxiety (Sturman et al., 2018), and locomotion can be used to assay sickness and malaise (Engeland et al., 2001). No significant differences were observed in total rearing events or total rearing time for all treatment groups. However, a significant difference in total distance traveled was observed between the vehicle and both the functionalized and non-functionalized soot treatment groups. If the soot treatment causes pronounced health problems, we might expect large decreases in the amount of time rearing or locomotion behavior. As we did not observe pronounced changes in behaviors, this suggest the soot treatment does not cause any generalized decreases in health.

Functionalized soot decreases the number of olfactory progenitor cells

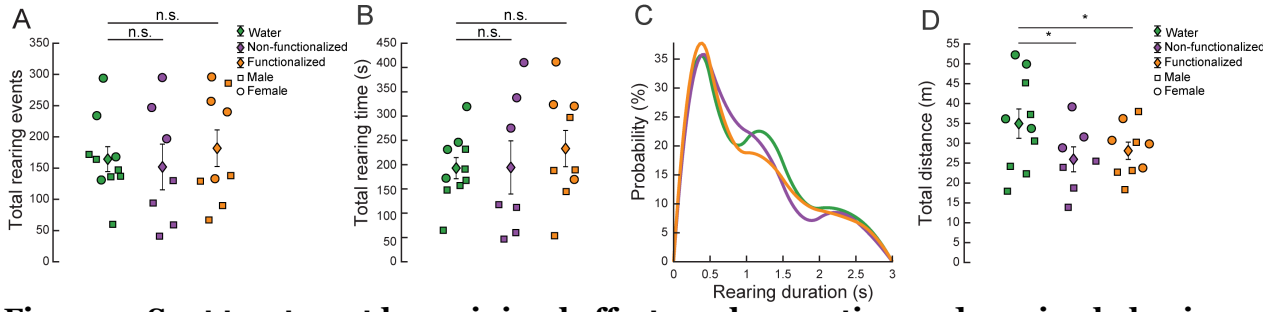

Figure 4: Soot treatment has minimal effects on locomotion and rearing behavior Comparisons of the effects of vehicle, non-functionalized, and functionalized soot on spontaneous rearing and locomotion behaviors over 20 minutes. The data from each individual mouse is shown as a square (males) or circle (females). The mean of each group is shown as a diamond, standard deviation is denoted with error bars. A) Plot of total number of rearing events for each treatment type. There was no significant difference in the number of rearing events between the control and either of the soot treatment groups ($p < 0.62$ non-functionalized, $p < 0.63$ functionalized). B) Plot of total rearing time. There was no significant difference in the total rearing time between groups ($p < 0.94$ non-functionalized, $p < 0.33$ functionalized). C) Probability distribution of individual rearing event durations for each of the treatment groups. (D) Plot of total distance travelled by each mouse. Treatment with non-functionalized soot ($p < 0.02$) and functionalized soot ($p < 0.05$) both significantly decreased the total distance traveled relative to the vehicle treated group.

As we saw no obvious changes in olfactory sensory neurons and their axons, we then asked how soot treatment might affect other cell types in the nasal epithelium, particularly the progenitor cells that directly and indirectly give rise to olfactory sensory neurons. If these cells are damaged, then this could lead to a long-term decline in the number of OSNs as the animals age. We used immunofluorescence staining of the neuroepithelium to visualize changes in progenitor cells (Fig. 5A-B). The expression of the anti-Pax6 or anti-p63 primary antibody in the neuroepithelium was quantified to assess any disruptions in the number of globular basal cells (GBCs) or horizontal basal cells (HBCs), respectively (Fig. 5C-G). In the neuroepithelium, compared to the non-functionalized and vehicle treatments, a significant decrease in the number of Pax6^{+} cells was observed following the one-month treatment with functionalized soot (Fig. 5C-F). This decrease in Pax6^{+} cells implies a decrease in the pool of OSN progenitor cells. However, no significant differences in the number of p63^{+} cells were observed in the neuroepithelium for any of the treatment types (Fig. 5C-E, G), indicating no response by the HBCs following soot

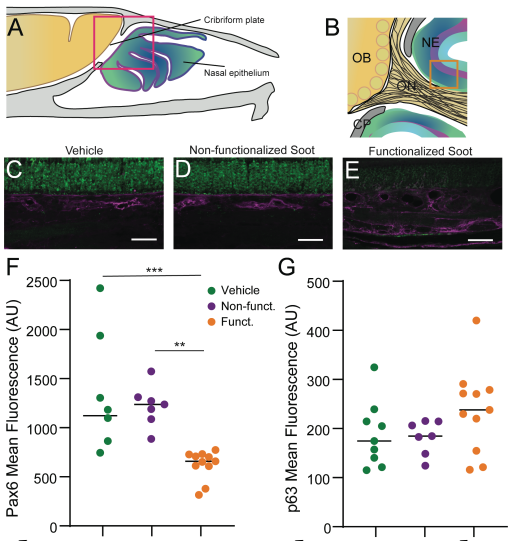

Figure 5: Functionalized soot treatment decreases the number of Pax6^{+} GBC olfactory progenitor cells

A) Schematic of the sagittal plane of the mouse cranial and nasal cavities. Olfactory nerve (ON), neuroepithelium (NE), cribriform plate (CP), and olfactory bulb (OB). Glomeruli are yellow circles. B) Sagittal view of the area within the pink box in A. C-E) Immunofluorescent staining of an area enclosed by the orange box. Pax6 is shown in green and p63 is shown in magenta. Scale bar 250μm. C) Vehicle control. D) Non-functionalized soot. E) Functionalized soot. F) Quantification Pax6 fluorescence. Functionalized soot caused a decrease in Pax6 expression (one way ANOVA, $F(2,24) = 11.04$, $p < 0.0004$) relative to non-functionalized soot (post-hoc unpaired t-test, $t(24) = 3.572$, $p < 0.0046$) and vehicle control (post-hoc unpaired t-test, $t(24) = 4.266$, $p < 0.00008$). G) No significant difference between group means of p63 fluorescence (one-way ANOVA, $F(2,24) = 1.797$, $p < 0.19$).

exposure. Decreases in the number of GBCs could lead to decreases in the number of olfactory sensory neurons in the long term.

Discussion

In order to understand how air pollution might affect olfactory sensory neurons and their progenitor cells, we treated mice intranasally with surrogate soot-like particles that either had oxygen-functionalized surfaces or non-functionalized surfaces. We found that these compounds had minimal effects on behavior, the olfactory sensory nerve, or horizontal basal cells. However, oxygen functionalized soot greatly reduced the population of globular basal cells. Our results are consistent with many other studies that have found that oxidized soots are more cytotoxic than un-oxidized soots (Li et al., 2009; Holder et al., 2012; Pourkhesalian et al., 2015).

Our results suggest a potential model of how long-term exposure to air pollutants could drive anosmia and decreased CSF outflow into the nasal cavity (Fig. 6). Exposure to oxidized soot particles reduces the number of GBCs. As olfactory sensory neurons senesce, the reduced population of GBCs leads to incomplete replacement of OSNs. The decrease in OSNs could then potentially lead to decreases in olfactory sensitivity seen with exposure to air pollution (Ajmani et al., 2016a; Ajmani et al., 2016b; Hummel et al., 2017). The decrease in OSN axons could also reduce fluid outflow through the cribriform

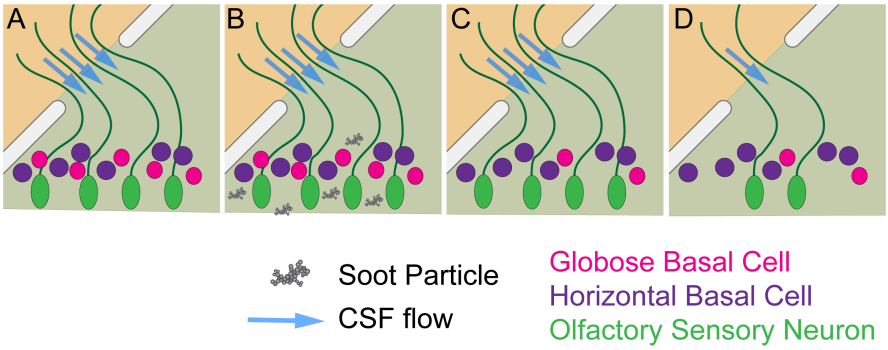

Figure 6: Potential impact of decreased number of GBCs on CSF outflow
A) Normally, cerebrospinal fluid drains (between olfactory sensory neuron axons) out of the cranial compartment (upper left) into the nasal compartment. Exposure to oxidized soots (B) results in the death of GBCs (C). Decreases in the number of GBCs eventually leads to a decrease in the number of olfactory sensory neurons (D), as they are not replaced after they die, so there is less CSF draining out of the cribriform plate.

plate (Norwood et al., 2019), which may lead to slower CSF turnover and a buildup of toxic metabolites in the CSF, and potentially to development of neurodegenerative diseases (Iliff et al., 2012). We emphasize though this explanation unites many disparate observations, it is nonetheless speculative.

There are several limitations to our study. We do not know the mechanism by which oxygen functionalized soot preferentially damages GBCs. It could be that oxygen functionalized soot is more prone to accumulating in the nasal epithelium (Fig. 2), enhancing their toxic effects. Only a single kind of air pollutant was tested here, and other known pollutants (such as heavy metals) could have different or synergistic effects (Calderón-Garcidueñas et al., 2002; Costa et al., 2020). Finally, we only looked at relatively acute effects of exposure, and longer-term exposure may have different effects.

Author contributions: JNN, APG, KLT and LFP performed experiments, JNN, APG and KLT analyzed data, JNN, RVW and PJD designed the experiments and wrote the manuscript with input from all authors.

References

Absinta M, Ha SK, Nair G, Sati P, Luciano NJ, Palisoc M, Louveau A, Zaghloul KA, Pittaluga S, Kipnis J, Reich DS (2017) Human and nonhuman primate meninges harbor lymphatic vessels that can be visualized noninvasively by MRI. Elife 6.

Ajmani GS, Suh HH, Pinto JM (2016a) Effects of Ambient Air Pollution Exposure on Olfaction: A Review. Environ Health Perspect 124:1683-1693.

Ajmani GS, Suh HH, Wroblewski KE, Kern DW, Schumm LP, McClintock MK, Yanosky JD, Pinto JM (2016b) Fine particulate matter exposure and olfactory dysfunction among urban-dwelling older US adults. Environ Res 151:797-803.

Albeck MJ, Skak C, Nielsen PR, Olsen KS, Borgesen SE, Gjerris F (1998) Age dependency of resistance to cerebrospinal fluid outflow. J Neurosurg 89:275-278.

Aspelund A, Antila S, Proulx ST, Karlsen TV, Karaman S, Detmar M, Wiig H, Alitalo K (2015) A dural lymphatic vascular system that drains brain interstitial fluid and macromolecules. J Exp Med 212:991-999.

Atanasova B, Graux J, El Hage W, Hommet C, Camus V, Belzung C (2008) Olfaction: a potential cognitive marker of psychiatric disorders. Neurosci Biobehav Rev 32:1315-1325.

Benveniste H, Lee H, Volkow ND (2017) The Glymphatic Pathway: Waste Removal from the CNS via Cerebrospinal Fluid Transport. Neuroscientist 23:454-465.

Bird DJ, Murphy WJ, Fox-Rosales L, Hamid I, Eagle RA, Van Valkenburgh B (2018) Olfaction written in bone: cribriform plate size parallels olfactory receptor gene repertoires in Mammalia. Proc Biol Sci 285.

Boulton M, Young a, Hay J, Armstrong D, Flessner M, Schwartz M, Johnston M (1996) Drainage of CSF through lymphatic pathways and arachnoid villi in sheep: measurement of 125I-albumin clearance. Neuropathology and applied neurobiology 22:325-333.

Bradbury MW, Cserr HF, Westrop RJ (1981) Drainage of cerebral interstitial fluid into deep cervical lymph of the rabbit. The American journal of physiology 240:F329-F336.

Brann JH, Firestein SJ (2014) A lifetime of neurogenesis in the olfactory system. Front Neurosci 8:182.

Buoli M, Grassi S, Caldiroli A, Carnevali GS, Mucci F, Iodice S, Cantone L, Pergoli L, Bollati V (2018) Is there a link between air pollution and mental disorders? Environ Int 118:154-168.

Burnett R et al. (2018) Global estimates of mortality associated with long-term exposure to outdoor fine particulate matter. Proc Natl Acad Sci U S A 115:9592-9597.

Calderon-Garciduenas L, Maronpot RR, Torres-Jardon R, Henriquez-Roldan C, Schoonhoven R, Acuna-Ayala H, Villarreal-Calderon A, Nakamura J, Fernando R, Reed W, Azzarelli B, Swenberg JA (2003) DNA damage in nasal and brain tissues of canines exposed to air pollutants is associated with evidence of chronic brain inflammation and neurodegeneration. Toxicol Pathol 31:524-538.

Calderón-Garcidueñas L, Azzarelli B, Acuna H, Garcia R, Gambling TM, Osnaya N, Monroy S, del Tizapantzi MR, Carson JL, Villarreal-Calderon A, Rewcastle B (2002) Air pollution and brain damage. Toxicologic pathology 30:373-389.

Chen M, Reed RR, Lane AP (2019) Chronic Inflammation Directs an Olfactory Stem Cell Functional Switch from Neuroregeneration to Immune Defense. Cell Stem Cell.

Child KM, Herrick DB, Schwob JE, Holbrook EH, Jang W (2018) The Neuroregenerative Capacity of Olfactory Stem Cells Is Not Limitless: Implications for Aging. J Neurosci 38:6806-6824.

Cooper KW, Brann DH, Farruggia MC, Bhutani S, Pellegrino R, Tsukahara T, Weinreb C, Joseph PV, Larson ED, Parma V, Albers MW, Barlow LA, Datta SR, Di Pizio A (2020) COVID-19 and the Chemical Senses: Supporting Players Take Center Stage. Neuron 107:219-233.

Costa LG, Cole TB, Dao K, Chang YC, Coburn J, Garrick JM (2020) Effects of air pollution on the nervous system and its possible role in neurodevelopmental and neurodegenerative disorders. Pharmacol Ther 210:107523.

Croy I, Symmank A, Schellong J, Hummel C, Gerber J, Joraschky P, Hummel T (2014) Olfaction as a marker for depression in humans. J Affect Disord 160:80-86.

de Leon MJ, Li Y, Okamura N, Tsui WH, Saint Louis LA, Glodzik L, Osorio RS, Fortea J, Butler T, Pirraglia E, Fossati S, Kim HJ, Carare RO, Nedergaard M, Benveniste H, Rusinek H (2017) CSF clearance in Alzheimer Disease measured with dynamic PET. J Nucl Med.

Dennison JR, Holtz M, Swain M (1996) Raman Spectroscopy of Carbon Materials. Spectroscopy 11:38-45.

Donnet JB (1993) Carbon black: science and technolog: CRC Press.

Doty RL (1989) Influence of age and age-related diseases on olfactory function. Ann N Y Acad Sci 561:76-86.

Engeland CG, Nielsen DV, Kavaliers M, Ossenkopp KP (2001) Locomotor activity changes following lipopolysaccharide treatment in mice: a multivariate assessment of behavioral tolerance. Physiol Behav 72:481-491.

Forman HJ, Finch CE (2018) A critical review of assays for hazardous components of air pollution. Free Radic Biol Med 117:202-217.

Gogos JA, Osborne J, Nemes A, Mendelsohn M, Axel R (2000) Genetic Ablation and Restoration of the Olfactory Topographic Map. Cell 103:609-620.

Growdon ME, Schultz AP, Dagley AS, Amariglio RE, Hedden T, Rentz DM, Johnson KA, Sperling RA, Albers MW, Marshall GA (2015) Odor identification and Alzheimer disease biomarkers in clinically normal elderly. Neurology 84:2153-2160.

Hasegawa-Ishii S, Shimada A, Imamura F (2019) Neuroplastic changes in the olfactory bulb associated with nasal inflammation in mice. J Allergy Clin Immunol 143:978-989 e973.

Holder AL, Carter BJ, Goth–Goldstein R, Lucas D, Koshland CP (2012) Increased cytotoxicity of oxidized flame soot. Atmospheric Pollution Research 3:25-31.

Hong W, Kennedy A, Burgos-Artizzu XP, Zelikowsky M, Navonne SG, Perona P, Anderson DJ (2015) Automated measurement of mouse social behaviors using depth sensing, video tracking, and machine learning. Proc Natl Acad Sci U S A 112:E5351-5360.

Hummel T et al. (2017) Position paper on olfactory dysfunction. Rhinol Suppl 54:1-30.

Iliff JJ, Wang M, Liao Y, Plogg BA, Peng W, Gundersen GA, Benveniste H, Vates GE, Deane R, Goldman SA, Nagelhus EA, Nedergaard M (2012) A Paravascular Pathway Facilitates CSF Flow Through the Brain Parenchyma and the Clearance of Interstitial Solutes, Including Amyloid β. Science translational medicine 4:147ra111-147ra111.

Kohli P, Soler ZM, Nguyen SA, Muus JS, Schlosser RJ (2016) The Association Between Olfaction and Depression: A Systematic Review. Chem Senses 41:479-486.

Kundu S, Wang Y, Xia W, Muhler M (2008) Thermal Stability and Reducibility of Oxygen-Containing Functional Groups on Multiwalled Carbon Nanotube Surfaces: A Quantitative High-Resolution XPS and TPD/TPR Study. The Journal of Physical Chemistry C 112:16869-16878.

Li Q, Wyatt A, Kamens RM (2009) Oxidant generation and toxicity enhancement of aged-diesel exhaust. Atmospheric Environment 43:1037-1042.

Li Q, Shang J, Zhu T (2013) Physicochemical characteristics and toxic effects of ozone-oxidized black carbon particles. Atmospheric Environment 81:68-75.

Liberia T, Martin-Lopez E, Meller SJ, Greer CA (2019) Sequential Maturation of Olfactory Sensory Neurons in the Mature Olfactory Epithelium. eNeuro 6.

Louveau A, Da Mesquita S, Kipnis J (2016) Lymphatics in Neurological Disorders: A Neuro-Lympho-Vascular Component of Multiple Sclerosis and Alzheimer's Disease? Neuron 91:957-973.

Ma Q, Ineichen BV, Detmar M, Proulx ST (2017) Outflow of cerebrospinal fluid is predominantly through lymphatic vessels and is reduced in aged mice. Nat Commun 8:1434.

Ma Q, Ries M, Decker Y, Muller A, Riner C, Bucker A, Fassbender K, Detmar M, Proulx ST (2018) Rapid lymphatic efflux limits cerebrospinal fluid flow to the brain. Acta Neuropathol.

Mollanji R, Bozanovic-Sosic R, Zakharov A, Makarian L, Johnston MG (2002) Blocking cerebrospinal fluid absorption through the cribriform plate increases resting intracranial pressure. Am J Physiol Regul Integr Comp Physiol 282:R1593-1599.

Murphy C (2019) Olfactory and other sensory impairments in Alzheimer disease. Nature reviews Neurology 15:11-24.

Nagra G, Koh L, Zakharov A, Armstrong D, Johnston M (2006) Quantification of cerebrospinal fluid transport across the cribriform plate into lymphatics in rats. American journal of physiology Regulatory, integrative and comparative physiology 291:R1383-R1389.

Nedergaard M (2013) Neuroscience. Garbage truck of the brain. Science 340:1529-1530.

Norwood JN, Zhang Q, Card D, Craine A, Ryan TM, Drew PJ (2019) Anatomical basis and physiological role of cerebrospinal fluid transport through the murine cribriform plate. Elife 8.

Ottaviano G, Frasson G, Nardello E, Martini A (2016) Olfaction deterioration in cognitive disorders in the elderly. Aging Clin Exp Res 28:37-45.

Pant P, Habib G, Marshall JD, Peltier RE (2017) PM2.5 exposure in highly polluted cities: A case study from New Delhi, India. Environ Res 156:167-174.

142 Parent P, Laffon C, Marhaba I, Ferry D, Regier TZ, Ortega IK, Focsa C (2016) Nanoscale characterization of aircraft soot: A high-resolution transmission electron microscopy, Raman spectroscopy, X-ray
144 photoelectron and near-edge X-ray absorption spectroscopy study. Carbon 101:86-100.

Peters R, Ee N, Peters J, Booth A, Mudway I, Anstey KJ (2019) Air Pollution and Dementia: A Systematic
146 Review. J Alzheimers Dis 70:S145-S163.

Pourkhesalian AM, Stevanovic S, Rahman MM, Faghihi EM, Bottle SE, Masri AR, Brown RJ, Ristovski
148 ZD (2015) Effect of atmospheric aging on volatility and reactive oxygen species of biodiesel exhaust nano-particles. Atmospheric Chemistry and Physics 15:9099-9108.

150 Rahayel S, Frasnelli J, Joubert S (2012) The effect of Alzheimer's disease and Parkinson's disease on olfaction: a meta-analysis. Behav Brain Res 231:60-74.

152 Rattanavaraha W, Rosen E, Zhang H, Li Q, Pantong K, Kamens RM (2011) The reactive oxidant potential of different types of aged atmospheric particles: An outdoor chamber study. Atmospheric
154 Environment 45:3848-3855.

Roberts RO, Christianson TJ, Kremers WK, Mielke MM, Machulda MM, Vassilaki M, Alhurani RE, Geda
156 YE, Knopman DS, Petersen RC (2016) Association Between Olfactory Dysfunction and Amnestic Mild Cognitive Impairment and Alzheimer Disease Dementia. JAMA Neurol 73:93-101.

158 Romanos GE, Likodimos V, Marques RRN, Steriotis TA, Papageorgiou SK, Faria JL, Figueiredo JL, Silva AMT, Falaras P (2011) Controlling and Quantifying Oxygen Functionalities on Hydrothermally
160 and Thermally Treated Single-Wall Carbon Nanotubes. The Journal of Physical Chemistry C 115:8534-8546.

162 Sadezky A, Muckenhuber H, Grothe H, Niessner R, Pöschl U (2005) Raman microspectroscopy of soot and related carbonaceous materials: Spectral analysis and structural information. Carbon
164 43:1731-1742.

Simon MJ, Iliff JJ (2016) Regulation of cerebrospinal fluid (CSF) flow in neurodegenerative,
166 neurovascular and neuroinflammatory disease. Biochim Biophys Acta 1862:442-451.

Stoquart-ElSankari S, Baledent O, Gondry-Jouet C, Makki M, Godefroy O, Meyer ME (2007) Aging effects on cerebral blood and cerebrospinal fluid flows. J Cereb Blood Flow Metab 27:1563-1572.

Sturman O, Germain PL, Bohacek J (2018) Exploratory rearing: a context- and stress-sensitive behavior recorded in the open-field test. Stress 21:443-452.

Tuinstra F, Koenig JL (1970) Raman Spectrum of Graphite. The Journal of Chemical Physics 53:1126-1130.

Vander Wal RL, Bryg VM, Hays MD (2011) XPS analysis of combustion aerosols for chemical composition, surface chemistry, and carbon chemical state. Anal Chem 83:1924-1930.

Wang Y, Xiong L, Tang M (2017) Toxicity of inhaled particulate matter on the central nervous system: neuroinflammation, neuropsychological effects and neurodegenerative disease. J Appl Toxicol 37:644-667.

Wilson RS, Arnold SE, Schneider JA, Boyle PA, Buchman AS, Bennett DA (2009) Olfactory impairment in presymptomatic Alzheimer's disease. Ann N Y Acad Sci 1170:730-735.

Yoo SJ, Son G, Bae J, Kim SY, Yoo YK, Park D, Baek SY, Chang KA, Suh YH, Lee YB, Hwang KS, Kim Y, Moon C (2020) Longitudinal profiling of oligomeric Abeta in human nasal discharge reflecting cognitive decline in probable Alzheimer's disease. Sci Rep 10:11234.

Zhang Q, Roche M, Gheres KW, Chaigneau E, Kedarasetti RT, Haselden WD, Charpak S, Drew PJ (2019) Cerebral oxygenation during locomotion is modulated by respiration. Nat Commun 10:5515.

Zíková N, Wang Y, Yang F, Li X, Tian M, Hopke PK (2016) On the source contribution to Beijing PM2.5 concentrations. Atmospheric Environment 134:84-95.